SCIENTIFIC REPORTS
nature research

Check for updates

OPEN

Intravoxel incoherent motion diffusion-weighted imaging to differentiate hepatocellular carcinoma from intrahepatic cholangiocarcinoma

Juan Peng[1,2,3], Jing Zheng[1], Cui Yang[1], Ran Wang[1], Yi Zhou[1], Yun-Yun Tao[1], Xue-Qin Gong[1], Wei-Cheng Wang[1,3], Xiao-Ming Zhang[1] & Lin Yang[1]✉

The present study aimed to explore the value of intravoxel incoherent motion diffusion-weighted imaging (IVIM-DWI) in differentiating hepatocellular carcinoma (HCC) from intrahepatic cholangiocarcinoma (ICC). This study included 65 patients with malignant hepatic nodules (55 with HCC, 10 with ICC), and 17 control patients with normal livers. All patients underwent IVIM-DWI scans on a 3.0T magnetic resonance imaging (MRI) scanner. The standard apparent diffusion coefficient (ADC), pure diffusion coefficient (D_{slow}), pseudo-diffusion coefficient (D_{fast}), and perfusion fraction (f) were obtained. Differences in the parameters among the groups were analysed using one-way ANOVA, with $p < 0.05$ indicating statistical significance. Receiver operating characteristic (ROC) curve analysis was used to compare the efficacy of each parameter in differentiating HCC from ICC. ADC, D_{slow}, D_{fast}, f significantly differed among the three groups. ADC and D_{slow} were significantly lower in the HCC group than in the ICC group, while D_{fast} was significantly higher in the HCC group than in the ICC group; f did not significantly differ between the HCC and ICC groups. When the cut-off values of ADC, D_{slow}, and D_{fast} were 1.27×10^{-3} mm^2/s, 0.81×10^{-3} mm^2/s, and 26.04×10^{-3} mm^2/s, respectively, their diagnostic sensitivities for differentiating HCC from ICC were 98.18%, 58.18%, and 94.55%, their diagnostic specificities were 50.00%, 80.00%, and 80.00%, and their areas under the ROC curve (AUCs) were 0.687, 0.721, and 0.896, respectively. D_{fast} displayed the largest AUC value. IVIM-DWI can be used to differentiate HCC from ICC.

Hepatocellular carcinoma (HCC) and intrahepatic cholangiocarcinoma (ICC) are the common primary liver cancers (PLCs) worldwide. Because the therapeutic strategies and prognosis of HCC and ICC are quite different, accurate differentiation is very important[1]. However, distinguishing HCC from ICC by using conventional imaging methods is often fairly difficult because these diseases have similar imaging features[2]. Diffusion-weighted imaging (DWI) is a quantitative method used to detect the metabolic functions of live tissues by measuring the apparent diffusion coefficient (ADC)[3–5]. However, DWI cannot distinguish between the diffusion of water molecules and the perfusion of blood. Specifically, intravoxel incoherent motion diffusion-weighted imaging (IVIM-DWI) can simultaneously quantify the diffusion of water molecules and microcirculation perfusion in living tissues, and thus compensates for the limitations of traditional DWI[6–9]. Among the parameters used by IVIM-DWI, the pure diffusion coefficient (D_{slow}) reflects the diffusion of pure water molecules, the pseudo-diffusion coefficient (D_{fast}) reflects the diffusion movement of capillary microcirculation perfusion, and the perfusion fraction (f) represents the volume ratio between the perfusion effect of local microcirculation and the overall diffusion effect.

[1]Department of Radiology, Medical Research Center, Affiliated Hospital of North Sichuan Medical College, Nanchong, Sichuan, 637000, P. R. China. [2]Department of Radiology, Sichuan Provincial People's Hospital Jinniu Hospital,Chengdu Jinniu District People's Hospital, Chengdu, Sichuan, 610007, P. R. China. [3]These authors contributed equally: Juan Peng and Wei-Cheng Wang. ✉e-mail: linyangmd@163.com

	ADC	D_{slow}	D_{fast}	f
HCC group	1.01 ± 0.19^a	0.81 ± 0.18^a	35.36 ± 6.77^a	0.18 ± 0.06^a
ICC group	1.17 ± 0.27^b	0.98 ± 0.22^b	24.16 ± 5.87^b	0.15 ± 0.03^a
Control group	1.22 ± 0.03^b	1.10 ± 0.05^b	65.32 ± 14.93^c	0.22 ± 0.03^b
F	10.896	20.327	90.684	6.456
p	0.000	0.000	0.000	0.003

Table 1. Comparison of the IVIM-DWI parameters among HCC, ICC, and control groups. Note: The units for the ADC, D_{slow}, and D_{fast} are all 10^{-3} mm^2/s. Different letters at the upper right corners of the numbers indicate significant difference between the groups.

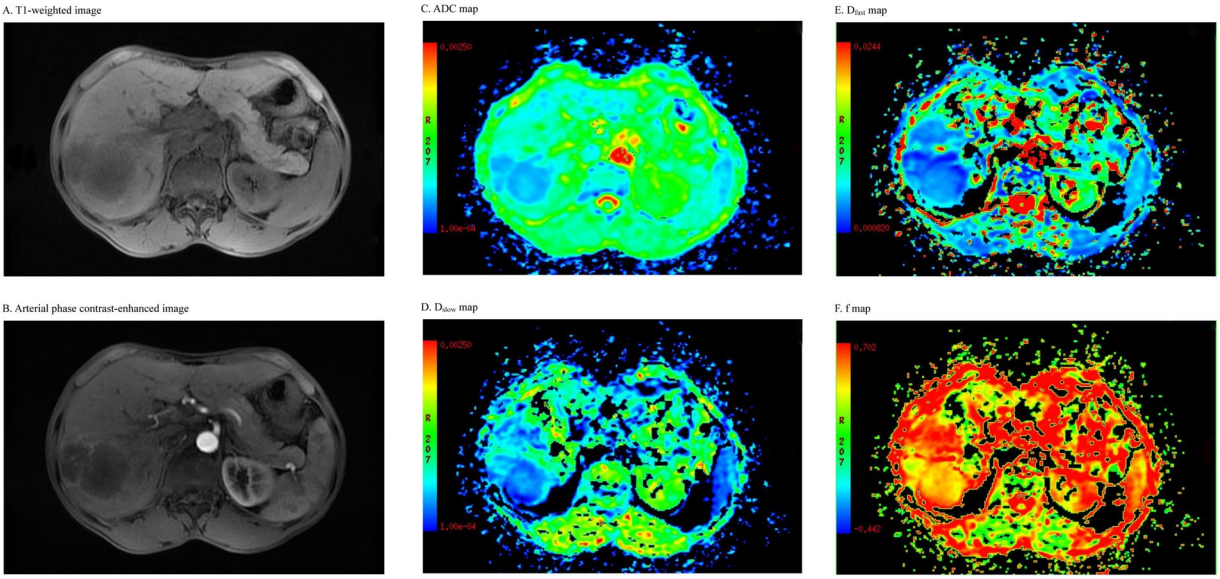

Figure 1. Axial MRI images of an HCC patient. (**A**): A T1-weighted image shows a hypointensive lesion in the right lobe of the liver. (**B**): An arterial phase contrast-enhanced image shows an inhomogeneous enhanced lesion. (**C**): ADC map. (**D**): D_{slow} map. (**E**): D_{fast} map. (**F**): f map.

IVIM-DWI technology has been applied to the liver with the primary goals of identifying benign and malignant hepatic nodules[10–18], determining histologic grades[19–21], assessing the treatment response of HCC[22–25], grading cirrhosis[11,26–34] and evaluating non-alcoholic fatty liver disease[35–37]. However, the application of IVIM-DWI in the differential diagnosis of malignant nodules with different pathological properties in the liver has been rarely explored. The aim of the present study was to explore the value of IVIM-DWI in differentiating HCC from ICC.

Materials and Methods

Patients. The present study was approved by the Ethics of affiliated hospital of north Sichuan medical college, written informed consent was obtained for all individual participants, and all methods were performed in accordance with the relevant guidelines and regulations. Sixty-five patients with PLCs were enrolled in this study, including 52 males and 13 females, with ages ranging from 18 to 78 years and an average age of 51.2 ± 14.6 years. All patients underwent surgery, and their tumour statuses were confirmed by pathological evaluation. Normal liver tissues from another 17 patients served as the control group.

MRI. Using a GE Discovery MR750 3.0 T superconducting MRI scanner and a body-specific 32-channel phased-array coil (GE Medical Systems, Milwaukee, Wis., USA), all patients successively underwent axial breath-hold fat-suppressed T1-weighted imaging (T1WI), respiratory-triggered fat-suppressed T2-weighted imaging (T2WI), IVIM-DWI, and multiphase dynamic contrast-enhanced MRI. Before the scan, the patients fasted for 4 h and went through respiratory training. The scan covered the area from the top of the diaphragm to the lower edge of the liver (a scan of the entire liver). The IVIM-DWI sequence was selected based on nine different b-values (b = 0, 20, 40, 80, 100, 200, 400, 800, and 1,000 s/mm^2) with a repetition time/echo time (TR/TE) of 3,529 ms/60.8 ms, matrix of 128 × 160, field of view (FOV) of 36 cm × 36 cm − 40 cm × 40 cm and layer thickness/layer spacing of 5 mm/0.5 mm. During the multiphase dynamic contrast-enhanced MRI scan, the contrast agent Gd-DTPA (Bayer AG, Mullerstrasse 178, Berlin-Wedding 13353, Germany) was intravenously injected into the dorsal hand vein of each patient at a speed of 2.5 ml/s and a dose of 0.2 ml/kg. After the injection of the contrast agent, images were collected in the following phases: hepatic arterial phase, portal venous phase, late portal venous phase, and delayed phase (axial and coronal planes).

Parameters	Cut-off	Sensitivity (%)	Specificity (%)	AUC	95%CI
ADC	1.27	98.18	50.00	0.687	0.469–0.906
D_{slow}	0.81	58.18	80.00	0.721	0.557–0.885
D_{fast}	26.04	94.55	80.00	0.896	0.782–1.000

Table 2. The diagnostic performance of the IVIM-DWI parameters for the characterization of malignant liver nodules. Note: 95%CI: 95% confidence interval.

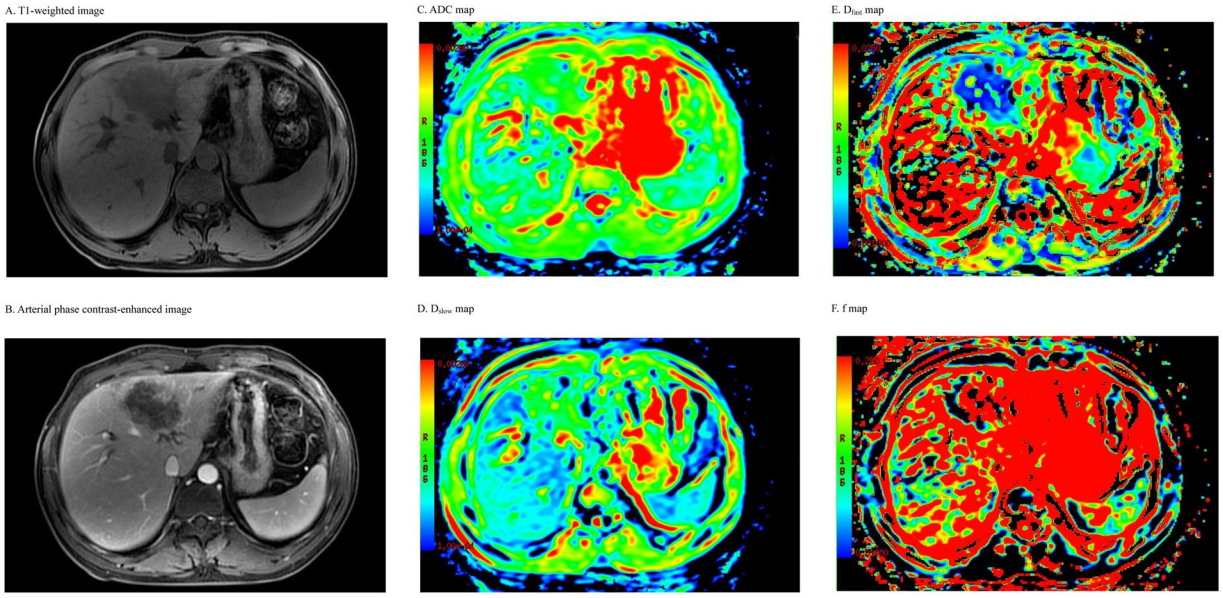

Figure 2. MR images of an ICC patient. (**A**): A T1-weighted image shows a hypointense lesion in the left lobe of the liver. (**B**): An arterial phase contrast-enhanced image shows an inhomogeneous enhanced lesion with biliary obstruction. (**C**): ADC map. (**D**): D_{slow} map. (**E**): D_{fast} map. (**F**): f map.

Data measurement. The images were transferred to the GE ADW4.6 post-processing workstation (GE Medical Systems, Milwaukee, Wis., USA), and image analysis was performed using Function-MADC software (GE Medical Systems, Milwaukee, Wis., USA). Pseudo-colour maps of the standard ADC, D_{slow}, D_{fast}, and f were generated. Regions of interest (ROIs) were placed in the largest solid areas of the lesions (avoiding regions of necrosis and haemorrhage in the tumours), and the IVIM-DWI parameters were measured.

Statistical analysis. All data were subjected to statistical analysis using SPSS 21.0 software. One-way ANOVA was used to analyse the differences in the parameters among different groups. When $p < 0.05$, the difference was considered statistically significant. The receiver operating characteristic (ROC) curve was used to compare the efficacy of each parameter in differentiating HCC from ICC.

Results

Among the 65 cases of PLCs, 55 were HCCs, and 10 were ICCs. Forty-eight patients had cirrhosis. The Child-Pugh score of liver function showed that 55 of the cases were grade A while 10 cases were grade B. The ADC, D_{slow}, D_{fast} and f all significantly differed among the HCC tissues, ICC tissues, and normal liver tissues (all $p < 0.05$). The ADC, D_{slow}, D_{fast}, and f of the HCC tissues were all lower than the ADC, D_{slow}, D_{fast} and f of the normal liver tissues (all $p < 0.05$). D_{fast} and f of the ICC tissues were lower than those of the normal liver tissues, but no significant differences were found in the other parameters between the two groups. The ADC and D_{slow} of HCC tissues were both significantly lower than those of ICC tissues (all $p < 0.05$), whereas D_{fast} of the HCC tissues was significantly higher than that of the ICC tissues ($p < 0.05$). Additionally, the f did not significantly differ between the HCC and ICC tissues ($p > 0.05$). When the cut-off values of the ADC, D_{slow}, and D_{fast} were 1.27×10^{-3} mm^2/s, 0.81×10^{-3} mm^2/s, and 26.04×10^{-3} mm^2/s, respectively, their diagnostic sensitivities for differentiating HCC from ICC were 98.18%, 58.18%, and 94.55%, respectively, their diagnostic specificities were 50.00%, 80.00%, and 80.00%, respectively, and their area under the curve (AUC) values were 0.687, 0.721, and 0.896, respectively; Dfast displayed the largest AUC (Tables 1 and 2) (Figs. 1–3). Among the 55 cases of HCC, 18 were World Health Organization (WHO) grade I, 22 were grade II, and 15 were grade III. The ADC and D_{slow} of HCC were significantly negatively correlated with the histological grades of the lesions (all $p < 0.05$), and the f of HCC was significantly positively correlated with the histological grades of the corresponding lesions (all $p < 0.05$).

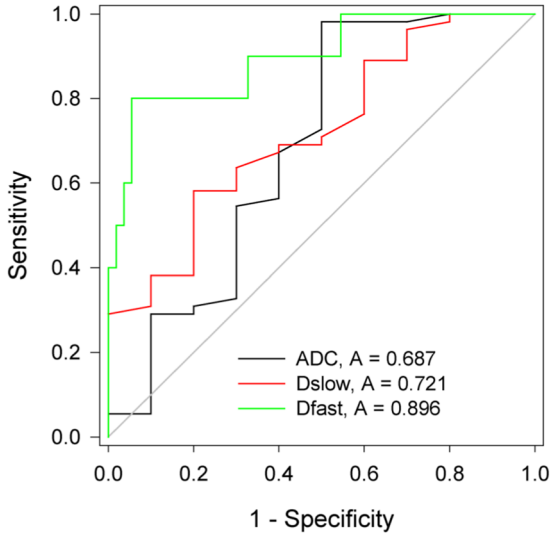

Figure 3. Receiver operating characteristic (ROC) curves of the IVIM-DWI parameters for differentiating HCC and ICC. The area under the curve (AUC) for D_{fast} was higher than those for the ADC and D_{slow}.

Discussion

IVIM-DWI acquires DWI images with multiple b-values and uses a bi-exponential pattern to extract quantitative information that reflects local tissue water molecule diffusion and microcirculation perfusion[6–9]. The application of IVIM-DWI to identify benign and malignant hepatic nodules has been proven to be important by previous researchers[10–18]. However, studies on the differential diagnosis of malignant hepatic nodules with different pathological properties by IVIM-DWI are very limited[10,17,38]. Watanabe H *et al.*[12] performed IVIM-DWI scans on a total of 120 hepatic nodules in 74 patients. The results showed that the true molecular-diffusion coefficient (D) and ADC of malignant nodules were significantly lower than those of benign nodules. The D and ADC of hepatic cysts were higher than those of hemangiomas, but the D and ADC did not differ between metastasis and HCC. The ADC of benign and malignant lesions had significantly greater AUCs than the D of the two types of lesions. Choi IY *et al.*[17] performed IVIM-DWI scanning of 161 liver nodule cases. The results showed that the D_{slow} values of HCC were obviously lower than those of ICC, and the f values of HCC were higher than those of ICC and metastasis. No differences were found among the ADC values of malignant nodules with different pathological properties. Among all of the parameters used to identify malignant nodules, D_{slow} displayed the largest AUC, and there were significant positive correlations between the f value and the enhancement fraction and between the f value and the relative enhancement. A study by Wei *et al.*[38] found that the ADC and D_{slow} can be beneficial for the differential diagnosis of HCC and ICC. D_{slow} showed a better discriminatory ability than the ADC, whereas D_{fast} and f displayed no differentiating power for ICC and HCC.

Data obtained from our study found significant differences among some of the IVIM-DWI parameters, including ADC, D_{slow}, and D_{fast} between HCC and ICC. The ADC and D_{slow} of HCC tissues were obviously lower than those of ICC tissues, which is consistent with the results reported by Choi[17] and Wei *et al.*[38]. The D_{fast} value of HCC tissues was significantly higher than that of ICC tissues, which may be associated with the rich blood supply inherent to HCC, while the blood supply of ICC is poor[39]. This result was not observed by Wei *et al.*[38]. The differential efficacy of D_{fast} for malignant hepatic nodules with different pathological features is higher than those of the ADC and D_{slow}, suggesting that D_{fast} can better reflect the changes in the tissue microstructure compared to the ADC and D_{slow}. No significant differences in the f values were found between HCC and ICC in this study in contrast to D_{fast}, which reflects changes in tissue perfusion. This might be because the D_{fast} value and the f value represent different aspects of perfusion, with D_{fast} representing the flow rate of blood in the microvessels and the f value representing the blood-carrying capacity of the capillaries[40].

Most studies have reported no differences in the IVIM-DWI parameters between HCC and liver metastases[12,41]. However, Choi *et al.*[17] reported that the f value of HCC tissue is higher than that of metastatic tissue. The primary results from our study demonstrated that except for the slightly higher D_{fast} values in HCC than those in metastatic cancer, the other parameters, including the ADC, D_{slow}, and f, showed no difference between HCC and metastatic cancer. These inconsistencies could be associated with the different primary lesions and the altered cell density and microcirculation in the metastatic lesions.

Woo *et al.*[19] acquired DWI scans of 42 HCC cases based on eight selected b-values (0–800 s/mm^2). The results showed that the diffusion coefficient (D) and ADC of high-grade HCC were significantly lower than those of low-grade HCC. Both the D and ADC were significantly associated with the pathological grades of the tumours. Regarding high or low grades of HCC, the AUC of the D value was larger than that of the ADC value, and the percentage of arterial enhancement was associated with the f value. The results of the present study showed that the ADC and D_{slow} of HCC tissues are negatively correlated with the histological grades of the lesions, whereas the f is positively correlated with the histological grades of the lesions, suggesting that IVIM-DWI can be used to evaluate the preoperative histological grades of HCC. The findings of the present study are essentially consistent with the results reported by Woo *et al.*

IVIM-DWI assessment of liver nodules can be influenced by certain pathological conditions such as liver fibrosis. Studies have shown that cirrhosis leads to restricted water molecule diffusion and therefore reduced blood perfusion. Luciani *et al.*[34] discovered that compared with those of normal liver tissues, the ADC and D_{fast} of cirrhotic tissue were significantly lower, but D_{slow} and f remained similar among the two types of tissue. A report by Patel *et al.*[42] suggested that the ADC, D_{slow}, D_{fast}, and f were all lower in the cirrhotic group than those in the non-cirrhotic group. In this study, most patients in the HCC group had cirrhosis; thus, we used normal livers as negative controls. The results revealed that the ADC, D_{slow}, D_{fast}, and f of HCC tissues were lower than those of normal liver tissues.

In the IVIM-DWI model, multiple b-values are used to perform a double-exponential fit on the DWI signal, which requires at least four different b-values (including $b = 0$ s/mm^2) to complete the calculation of related parameters. In the application of IVIM-DWI, a considerable discrepancy was found in the selection of b-values by different researchers[43–49]. At present, the number of b-values used in most studies is approximately eight to 14[15,34,42,48]. In the IVIM-DWI model, when the selected b-value is high, the attenuation of the signal basically reflects the pure water molecule diffusion, but when a low b-value is selected, the attenuation of the signal is more sensitive to the perfusion effect of the local microcirculation capillaries. The higher the number of b-values is, the longer the image acquisition time required. Therefore, optimizing the number and distribution of b-values and reducing the errors of IVIM-DWI parameter measurement are very important. Dyvorne *et al.*[48] investigated the impact of the number of b-values on IVIM-DWI parameters through the comparison and analysis of 16 b-values and measurement results of four optimized b-values of a reference group. Their results indicated that the accuracy and repeatability of the IVIM-DWI parameters were not significantly affected, and the latter approach actually reduced the image acquisition time considerably. The b-values in our study were selected according to the considerations set forth in previous literature[17,45,49], and small adjustments were made in accordance with the practical situation of our unit. A total of nine b-values were selected, of which five were lower values. The time of collection was approximately 6 min and 30 s. In future research, the quantity and distribution of b-values should be selected based on the different tissues examined and optimized through in-depth research[43].

The present study has several limitations. First, a limited number of ICC cases compared to the number of HCC cases were included in the sample groups. As a next step, we will continue the study with an increased number of ICC cases. Second, this study did not examine difference between the IVIM-DWI parameters of benign liver lesions and those of malignant lesions or investigate differences in IVIM-DWI parameters between HCC and other liver malignancies, which will be studied in a related project in the future after more cases are collected. Third, the relationship between IVIM-DWI parameters and the prognosis of the patients was not analysed. We plan to follow-up the prognosis of the patients and carry out relevant analyses in subsequent work.

In conclusion, IVIM-DWI can provide quantitative information reflecting water molecule diffusion and microcirculation perfusion in the local tissue. Furthermore, IVIM-DWI can be used for the differential identification of malignant nodules with different pathological properties in the liver.

Received: 13 August 2019; Accepted: 20 April 2020;
Published online: 07 May 2020

References

1. Bridgewater, J. *et al*. Guidelines for the Diagnosis and Management of Intrahepatic Cholangiocarcinoma. *J. Hepatol.* **60**, 1268–1289 (2014).
2. Kim, S. Y. Preoperative Radiologic Evaluation of Cholangiocarcinoma. *Korean J. Gastroenterol.* **69**, 159–163 (2017).
3. Taouli, B. & Koh, D. M. Diffusion-Weighted MR Imaging of the Liver. *Radiology.* **254**, 47–66 (2010).
4. Li, S. P. & Padhani, A. R. Tumor Response Assessments with Diffusion and Perfusion MRI. *J. Magn. Reson. Imaging.* **35**, 745–763 (2012).
5. Min, J. H. *et al*. Detection of Recurrent Hepatocellular Carcinoma After Surgical Resection: Non-Contrast Liver MR Imaging with Diffusion-Weighted Imaging Versus Gadoxetic Acid-Enhanced MR Imaging. *Br. J. Radiol.* **91**, 20180177 (2018).
6. Le Bihan, D. *et al*. MR Imaging of Intravoxel Incoherent Motions: Application to Diffusion and Perfusion in Neurologic Disorders. *Radiology.* **161**, 401–407 (1986).
7. Yoon, J. H. *et al*. Evaluation of Hepatic Focal Lesions Using Diffusion-Weighted MR Imaging: Comparison of Apparent Diffusion Coefficient and Intravoxel Incoherent Motion-Derived Parameters. *J. Magn. Reson. Imaging* **39**, 276–285 (2014).
8. Ma, W. *et al*. Quantitative Parameters of Intravoxel Incoherent Motion Diffusion Weighted Imaging (IVIM-DWI): Potential Application in Predicting Pathological Grades of Pancreatic Ductal Adenocarcinoma. *Quant. Imaging Med. Surg.* **8**, 301–310 (2018).
9. Yang, K., Zhang, X. M., Yang, L., Xu, H. & Peng, J. Advanced Imaging Techniques in the Therapeutic Response of Transarterial Chemoembolization for Hepatocellular Carcinoma. *World J. Gastroenterol.* **22**, 4835–4847 (2016).
10. Zhu, L., Cheng, Q., Luo, W., Bao, L. & Guo, G. A Comparative Study of Apparent Diffusion Coefficient and Intravoxel Incoherent Motion-Derived Parameters for the Characterization of Common Solid Hepatic Tumors. *ActaRadiol* **56**, 1411–1418 (2015).
11. Li, Y. T. *et al*. Liver Intravoxel Incoherent Motion (IVIM) Magnetic Resonance Imaging: A Comprehensive Review of Published Data On Normal Values and Applications for Fibrosis and Tumor Evaluation. *Quant. Imaging Med. Surg.* **7**, 59–78 (2017).
12. Watanabe, H. *et al*. Characterizing Focal Hepatic Lesions by Free-Breathing Intravoxel Incoherent Motion MRI at 3.0 T. *ActaRadiol* **55**, 1166–1173 (2014).
13. Ichikawa, S. *et al*. Intravoxel Incoherent Motion Imaging of Focal Hepatic Lesions. *J. Magn. Reson. Imaging.* **37**, 1371–1376 (2013).
14. Doblas, S. *et al*. Determination of Malignancy and Characterization of Hepatic Type with Diffusion-Weighted Magnetic Resonance Imaging: Comparison of Apparent Diffusion Coefficient and Intravoxel Incoherent Motion-Derived Measurements. *Invest. Radiol.* **48**, 722–728 (2013).
15. Yamada, I., Aung, W., Himeno, Y., Nakagawa, T. & Shibuya, H. Diffusion Coefficients in Abdominal Organs and Hepatic Lesions: Evaluation with Intravoxel Incoherent Motion Echo-Planar MR Imaging. *Radiology* **210**, 617–623 (1999).
16. Luo, M., Zhang, L., Jiang, X. H. & Zhang, W. D. Intravoxel Incoherent Motion Diffusion-Weighted Imaging: Evaluation of the Differentiation of Solid Hepatic Lesions. *TranslOncol* **10**, 831–838 (2017).
17. Choi, I. Y. *et al*. Intravoxel Incoherent Motion Diffusion-Weighted Imaging for Characterizing Focaepatic Lesions: Correlation with Lesion Enhancement. *J. Magn. Reson. Imaging.* **45**, 1589–1598 (2017).
18. Wang, M. *et al*. Evaluation of Hepatic s Using Intravoxel Incoherent Motion Diffusion-Weighted MRI. *Med. SciMonit* **22**, 702–709 (2016).

19. Woo, S. *et al*. Intravoxel Incoherent Motion Diffusion-Weighted MR Imaging of Hepatocellular Carcinoma: Correlation with Enhancement Degree and Histologic Grade. *Radiology* **270**, 758–767 (2014).
20. Zhu, S. C. *et al*. Intravoxel Incoherent Motion Diffusion-Weighted Magnetic Resonance Imaging for Predicting Histological Grade of Hepatocellular Carcinoma: Comparison with Conventional Diffusion-Weighted Imaging. *World J. Gastroenterol.* **24**, 929–940 (2018).
21. Wei, Y. *et al*. Intravoxel Incoherent Motion Diffusion-Weighted Imaging for Assessment of Histologic Grade of Hepatocellular Carcinoma: Comparison of Three Methods for Positioning Region of Interest. *Eur. Radiol.* **29**, 535–544 (2019).
22. Peng, J. *et al*. Intravoxel Incoherent Motion Diffusion Weighted Imaging for the Therapeutic Response of Transarterial Chemoembolization for Hepatocellular Carcinoma. *J. Cancer Ther.* **10**, 591–601 (2019).
23. Lee, Y. *et al*. Intravoxel Incoherent Motion MRI for Monitoring the Therapeutic Response of Hepatocellular Carcinoma to Sorafenib Treatment in Mouse Xenograft Tumor Models. *ActaRadiol* **58**, 1045–1053 (2017).
24. Shirota, N. *et al*. Intravoxel Incoherent Motion MRI as a Biomarker of Sorafenib Treatment for Advanced Hepatocellular Carcinoma: A Pilot Study. *Cancer Imaging.* **16**, 1 (2016).
25. Server, S. *et al*. Intravoxel Incoherent Motion Parameters for Assessing the Efficiency of Locoregional Bridging Treatments before Liver Transplantation. *Transpl. Proc.* **51**, 2391–2396 (2019).
26. Lu, P. X. *et al*. Decreases in Molecular Diffusion, Perfusion Fraction and Perfusion-Related Diffusion in Fibrotic Livers: A Prospective Clinical Intravoxel Incoherent Motion MR Imaging Study. *PLoS One* **9**, e113846 (2014).
27. Yoon, J. H. *et al*. Evaluation of Hepatic Fibrosis Using Intravoxel Incoherent Motion in Diffusion-Weighted Liver MRI. *J. Comput. Assist. Tomogr.* **38**, 110–116 (2014).
28. Ichikawa, S. *et al*. MRI-based Staging of Hepatic Fibrosis: Comparison of Intravoxel Incoherent Motion Diffusion-Weighted Imaging with Magnetic Resonance Elastography. *J. Magn. Reson.Imaging.* **42**, 204–210 (2015).
29. Wu, C. H. *et al*. Assessing Hepatic Fibrosis: Comparing the Intravoxel Incoherent Motion in MRI with Acoustic Radiation Force Impulse Imaging in US. *Eur. Radiol.* **25**, 3552–3559 (2015).
30. Parente, D. B. *et al*. Intravoxel Incoherent Motion Diffusion Weighted MR Imaging at 3.0 T: Assessment of Steatohepatitis and Fibrosis Compared with Liver Biopsy in Type 2 Diabetic Patients. *PLoS One.* **10**, e125653 (2015).
31. Zhang, B. *et al*. Intravoxel Incoherent Motion MR Imaging for Staging of Hepatic Fibrosis. *PLoS One.* **11**, e147789 (2016).
32. Hu, F. *et al*. Liver Fibrosis: *In Vivo* Evaluation Using Intravoxel Incoherent Motion-Derived Histogram Metrics with Histopathologic Findings at 3.0 T. *AbdomRadiol* **42**, 2855–2863 (2017).
33. Chen, C. *et al*. Evaluation of Liver Fibrosis with a Monoexponential Model of Intravoxel Incoherent Motion Magnetic Resonance Imaging. *Oncotarget.* **9**, 24619–24626 (2018).
34. Luciani, A. *et al*. Liver Cirrhosis: Intravoxel Incoherent Motion MR Imaging–Pilot Study. *Radiology.* **249**, 891–899 (2008).
35. Murphy, P. *et al*. Associations Between Histologic Features of Nonalcoholic Fatty Liver Disease (NAFLD) and Quantitative Diffusion-Weighted MRI Measurements in Adults. *J. Magn. Reson.Imaging* **41**, 1629–1638 (2015).
36. Shin, H. J. *et al*. Liver Intravoxel Incoherent Motion Diffusion-Weighted Imaging for the Assessment of Hepatic Steatosis and Fibrosis in Children. *World J. Gastroenterol.* **24**, 3013–3020 (2018).
37. Guiu, B. *et al*. Intravoxel Incoherent Motion Diffusion-Weighted Imaging in Nonalcoholic Fatty Liver Disease: A 3.0-T MR Study. *Radiology.* **265**, 96–103 (2012).
38. Wei, Y. *et al*. Intrahepatic Cholangiocarcinoma in the Setting of HBV-related Cirrhosis: Differentiation with Hepatocellular Carcinoma by Using Intravoxel Incoherent Motion Diffusion-Weighted MR Imaging. *Oncotarget.* **9**, 7975–7983 (2018).
39. Kim, S. J. *et al*. Peripheral Mass-Forming Cholangiocarcinoma in Cirrhotic Liver. *AJR Am. J. Roentgenol.* **189**, 1428–1434 (2007).
40. Le Bihan, D. & Turner, R. The Capillary Network: A Link Between IVIM and Classical Perfusion. *Magn. Reson. Med.* **27**, 171–178 (1992).
41. Wu, H. *et al*. Meta-Analysis of Intravoxel Incoherent Motion Magnetic Resonance Imaging in Differentiating Focal Lesions of the Liver. *Medicine* **97**, e12071 (2018).
42. Patel, J. *et al*. Diagnosis of Cirrhosis with Intravoxel Incoherent Motion Diffusion MRI and Dynamic Contrast-Enhanced MRI Alone and in Combination: Preliminary Experience. *J. Magn. Reson. Imaging.* **31**, 589–600 (2010).
43. Lemke, A., Stieltjes, B., Schad, L. R. & Laun, F. B. Toward an Optimal Distribution of B Values for Intravoxel Incoherent Motion Imaging. *Magn. Reson. Imaging.* **29**, 766–776 (2011).
44. Lee, Y. *et al*. Intravoxel Incoherent Motion Diffusion-Weighted MR Imaging of the Liver: Effect of Triggering Methods On Regional Variability and Measurement Repeatability of Quantitative Parameters. *Radiology* **274**, 405–415 (2015).
45. Cohen, A. D., Schieke, M. C., Hohenwalter, M. D. & Schmainda, K. M. The Effect of Low B-Values On the Intravoxel Incoherent Motion Derived Pseudodiffusion Parameter in Liver. *Magn. Reson. Med.* **73**, 306–311 (2015).
46. Lee, J. T. *et al*. Cross-Sectional Investigation of Correlation Between Hepatic Steatosis and IVIM Perfusion On MR Imaging. *Magn. Reson. Imaging.* **30**, 572–578 (2012).
47. Wang, Y. *et al*. Dependence of Intravoxel Incoherent Motion Diffusion MR Threshold B-Value Selection for Separating Perfusion and Diffusion Compartments and Liver Fibrosis Diagnostic Performance. *ActaRadiol* **60**, 3–12 (2019).
48. Dyvorne, H., Jajamovich, G., Kakite, S., Kuehn, B. & Taouli, B. Intravoxel Incoherent Motion Diffusion Imaging of the Liver: Optimal B-Value Subsampling and Impact On Parameter Precision and Reproducibility. *Eur. J. Radiol.* **83**, 2109–2113 (2014).
49. Chevallier, O., Zhou, N., He, J., Loffroy, R. & Wang, Y. Removal of Evidential Motion-Contaminated and Poorly Fitted Image Data Improves IVIM Diffusion MRI Parameter Scan-Rescan Reproducibility. *ActaRadiol* **59**, 1157–1167 (2018).

Acknowledgements

This study was supported by the projects of the Department of Science and Technology of Sichuan Province (2016JY0105) and Department of Education of Sichuan Province (18ZB0222).

Author contributions

Juan Peng and Ran Wang conducted the measurements, analysed the results, and prepared the manuscript; Lin Yang wrote and revised the manuscript; Wei-Cheng Wang and Xiao-Ming Zhang designed the study; Jing Zheng, Cui Yang, Yi Zhou, Yun-Yun Tao and Xue-Qin Gong collected the data and edited the manuscript.

Competing interests

The authors declare no competing interests.

Additional information

Correspondence and requests for materials should be addressed to L.Y.

Reprints and permissions information is available at www.nature.com/reprints.